CORPUS PUBLISHERS

Journal of Mineral and Material Science (JMMS)

ISSN: 2833-3616

Volume 3 Issue 4, 2022

Article Information

Received date : December 13, 2022

Published date: December 20, 2022

*Corresponding author

Shashank Sharma, Department of Physics, Dr CV Raman University, Kota Bilaspur (CG), 495113, India

DOI: 10.54026/JMMS/1049

Keywords

Solid-State Synthesis; X-Ray Diffraction (XRD); Akermanite; Thermoluminescence (TL); $Ca_2MgSi_2O_7:Dy^{3+}$ Phosphor; Energy Dispersive X-Ray Spectroscopy (EDX)

Research Article

Significant Contribution of Deeper Traps for Long Afterglow Process in Synthesized Thermoluminescence Material

Shashank Sharma[1*] and Sanjay Kumar Dubey[2]

[1]*Department of Physics, Dr CV Raman University, Kota Bilaspur (CG), 495113, India*

[2]*Department of Physics, Dr. Radha Bai, Govt Navin Girls College, Raipur (CG), 492001, India*

Abstract

A promising candidate of long persistent $Ca_2MgSi_2O_7:Dy^{3+}$ phosphor sample was well sintered via traditional high temperature solid-state synthesis technique and characterized in terms of crystal structure, particle size, phase composition and TL trapping parameters have briefly discussed using X-Ray Diffraction (XRD), Field Emission Scanning Electron microscopy (FESEM), Energy Dispersive X-ray (EDX) Spectroscopy and TL-Dosimetry Reader techniques. The XRD results revealed that it has formed in a single phase and tetragonal crystallography (Akermanite crystal structure) with a space group $P\bar{4}21m$. All trapping parameters such as activation energy (E) (i.e. trap depth), order of kinetics (b) and frequency factor (s), and all these trapping parameters were calculated using Chen's glow curve method. In this present paper, structural & thermal properties of synthesized phosphor are discussed in detail. We have clearly observed that the trapped electrons in the crystal lattice site and the self-trapped hole that both are responsible for crystal growth process. Deeper traps are highly helpful for increasing the long persistent duration and afterglow process.

Introduction

Presently, great considerations are being addressed to the investigation of the melilite group compounds called sorosilicates, which has been recognized as the foremost for the valuable applications of long persistent mechanism. Some specific feature of the melilite compounds, due to extensively utilized as host material for both transition and Rare-Earth (RE) metal ions for remarkable applications such as LEDs, solar cells, flat panel displays and many more in optoelectronic devices [1]. Åkermanite ($Ca_2MgSi_2O_7$) is very important crystal structure with divalent T^1 cations as an end-member of the melilite group of silicates. The natural appearance is a more significant supporting mineral in basic formations such as magmatic and metamorphic rocks, meteorites as well as blast furnace slags [2]. Melilite-type phosphors have characterized general formula $X_2T_1T_2^2O_7$, with a large cation site (where X=lanthanides ions or Na, Ca, Ba, Sr, Pb), while (T^1=Al, Si, Mg, Zn) and (T^2=Si, Al, B, Ge) are often coordinated by oxygen ions. Basically, they have displayed quaternary (i.e. tetragonal) crystal structure with $P\bar{4}21m$ (113) space group. The two $[T^2O_4]$ tetrahedral sites are joined by corner to form $[T_2^2O_7]$ dimers. As a result, they are linked again to surrounding four $[T^1O_4]$ tetrahedral sites via bridging oxygen [3]. Compared with the aluminate phosphors, silicates based phosphors have fascinated more specific features with regard to superior chemical-thermal stabilities [4], excellent water resistant, varied luminescence color emission from blue to yellow regions [5], stable crystal-structure, robust captivation in near-UV region, cheaper, less synthesization time and abundant properties [6,7]. Afterglow process has previously been well investigated in melilite compounds. Basically, host materials play a pivotal role in the discovery of novel phosphors. Therefore, we suggest that the sintered Dy^{3+} doped $Ca_2MgSi_2O_7$ phosphor is a preferable long-persistent phosphor and novel TL material because rare earth dysprosium [Dy^{3+}] ions mainly act as trap centers [8]. The combination of host, do-pant and the optimum doping percentage of do-pant ions plays a remarkable role for creating luminescence-centers and helps in developing sensitive TL phosphor material [9]. Furthermore, it is very likely that Dy^{3+} rare-earth ions are included in the electron trapping process. As a result, when Dy^{3+} ions are added into the host crystal lattice by doping process, then the persistent emission is stronger. The vital matter of fact that two Dy^{3+} ions can clearly substitute the three ions of the host crystal lattice site and Dy^{3+} ions may increase the formation of defects which act as electron traps, as potential oxygen vacancies [10]. It can be clearly seen that the afterglow intensity is proportional to the trap's concentration located within the suitable trap depths because excited electrons or released holes are accumulated in these traps centers [11]. On the other hand, many studies of them have been carried out on the synthesis technique, long-lasting luminescence properties, and mechanism of various rare-earth-doped crystals and glasses [12]. Radiation dosimetry is the most significant use of TL phosphors. On understanding the mechanism, new luminous materials may be used in various ways. The fields of health physics, radiation protection, and personal monitoring all benefit from TL dosimetry. Materials have a high degree of sensitivity, low reliance on radiation energy, low fading, low threshold exposure, and good chemical and mechanical properties [13]. In order to completely restore, modify, regenerate, and maintain the damaged tissue in the human body, it is crucial to design biocompatible, bioactive, bioresorbable, and durable materials for orthopaedic and dental implants [14]. These materials must also be capable of tolerating significant stress and pressures. Apart from this, it is in great demand in the wide areas of applications such as plasma display panels, drug delivery systems, cancer therapy as well as bone tissue engineering. In this way, we will not be an exaggeration to say that the silicate-based bioceramics, including silicate bioglass and akermanite structured $Ca_2MgSi_2O_7$ ceramics are playing its leading role in the field of medical research as compared to other materials. In this paper, we report that the synthesis of $Ca_2MgSi_2O_7:Dy^{3+}$ phosphors by conventional solid-state reaction synthesis technique and its structural characterization on the basis of XRD, FESEM, and EDX spectroscopy. Studies of thermal properties have also been done on the basis of thermoluminescence (TL) spectra.

Experimental Analysis

Material Synthesis

A sample with the general formula $Ca_2MgSi_2O_7:Dy^{3+}$ was successfully synthesized via solid-state reaction synthesis technique (Figure 1). The initial precursor chemical reagents were $CaCO_3$ (AR), MgO (AR), SiO_2 (AR) and Dy_2O_3(AR) with very fewer amounts of H_3BO_3 added as flux. The only purpose behind taking flux was that it increases the reaction rate while keeping itself unchanged, which makes the process of sample preparation very fast. The raw materials were weighed stoichiometrically and mixed homogeneously with adding a few drops of acetone (CH_3COCH_3) in an agate-mortar & pestle for 2h. Thereafter, the mixture was transferred to alumina crucible and sintered at 1200 °C for 3hours under a weak reducing atmosphere, which was produced with the help of burning charcoal. Final phosphor was obtained in the form of white powder. The final products were obtained after cooling the powder sample in room temperature by natural cooling process. Such a way, the resultant powder sample was restored in an airtight and waterproof bottle for further structural and thermal characterization studies.

The chemical reaction process is given as follows:

$$8CaCO_3 + 4MgO + 8SiO_2{*}H_2O \rightarrow 4Ca_2MgSi_2O_7 + 8CO_2(\uparrow) + 8H_2O(\uparrow) + 3O_2(\uparrow) \quad (1)$$

$$8CaCO_3 + 4MgO + 8SiO_2{*}H_2O + 2Dy_2O_3 \rightarrow 4Ca_2MgSi_2O_7:Dy^{3+} + 8CO_2(\uparrow) + 8H_2O(\uparrow) + 3O_2(\uparrow) \quad (2)$$

The chemical reaction process involves the chemical decomposition of calcium carbonate [$CaCO_3$] to form calcium oxide [CaO] & carbon di oxide [CO_2]. When the temperature reaches higher than 950 °C (approximately) then this process is done which is shown according to this chemical reaction as below:

$$CaCO_3 \rightarrow CaO + CO_2 \ (T \geq 950\ ^\circ C) \quad (3)$$

Material Characterization

For crystal structure and phase identification, powder XRD patterns of the prepared samples were carried out with the help of Bruker D8 Advance powder X-Ray Diffraction (XRD) system with target Cu-K_α radiation (λ=1.5405 Å). A field emission scanning electron microscope (ZESIS (FESEM-centre, NIT Raipur, Chhattisgarh)) associated with EDX was used to take the surface morphology images of the prepared sample. Thermoluminescence (TL) glow curves were plotted between emitted TL intensity and the temperature of the sample with the help of daily routine PC-based TLD Reader (TL 1009I) setup (Pt. R. S. University Raipur (C.G.) India).

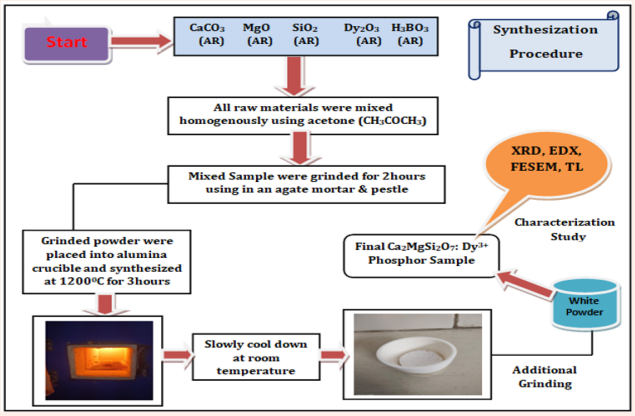

Figure 1: Synthesization procedure of powder sample.

Results and Discussion

XRD analysis

Some $Ca_2MgSi_2O_7$ based phosphors have been reported, which demonstrate the suitable host of $Ca_2MgSi_2O_7$ for phosphors [15,16]. Figure 2 displays the crystal structure and phase formation of un-doped & Dy^{3+} doped powder samples were well determined from the powder XRD patterns with target Cu-K_α radiation (λ=1.54056 Å). The XRD data were carried out in an extensive scattering angle range of (10°-80°) of Bragg angle 2θ. The crystal has a single phased, tetragonal crystallography system (akermanite phase structure) with cell volume is 303.663 (Å)3 and lattice cell parameters of a=7.8071 Å, b=7.8071 Å, c=4.9821 Å & α=β=γ=90°, belonging to space group $P\bar{4}2_1m$ space group (i.e. 113 space number and D^3_{2d} space group) and 24 atoms in the primitive unit cell [17]. Comparison of the recorded XRD peak positions and relative intensities of the synthesized powder samples were well clarified and better agreement with the help of standard JCPDS PDF file no. 77-1149 [18] and AMSCD Database Code 0008032 [19]. Comparing both powder samples, it can be clearly observed that all the diffraction peak positions have not changed even after addition of a fixed doping concentration of dysprosium activator ions. The crystal structure of the synthesized powder samples does not change from the fact that when dysprosium [Dy^{3+}]ions occupies calcium [Ca^{2+}] lattice sites within the host crystal lattice site. This is mainly because the ionic radii of Ca^{2+} ion sites are clearly captured by being close to the Dy^{3+} ionic radii.

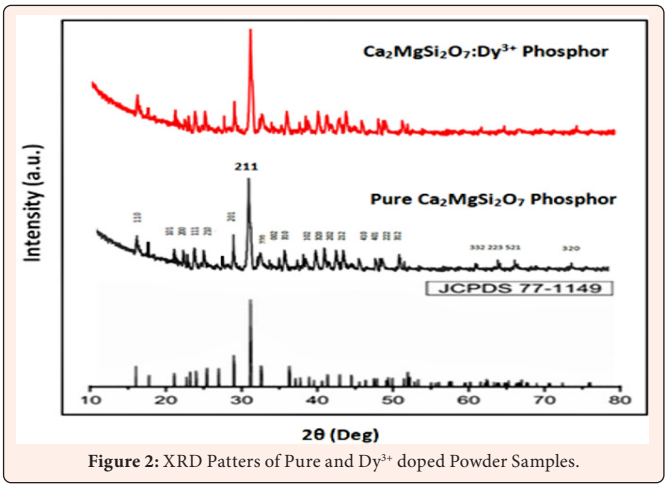

Figure 2: XRD Patters of Pure and Dy^{3+} doped Powder Samples.

Crystallite size (L) and crystal lattice strain (E): The crystallite size (D) and crystal lattice strain size component for the sintered powder samples are calculated with the help of the Debye Scherer's and W-H [Williamson-Hall Uniform Deformation Model (UDM)] plots [20-22]. Both, crystalline parameters were calculated from the XRD measurement. Figure 3 displays the W-H Plot of Un-doped & Dy^{3+} doped Sample.

a. **Debye-Scherer's formula**

This method is a very important and essential method from the point of view of estimating the crystal size clearly exists in the prepared samples.

$$L = \frac{0.94\lambda}{\beta \cos\theta} \quad (4)$$

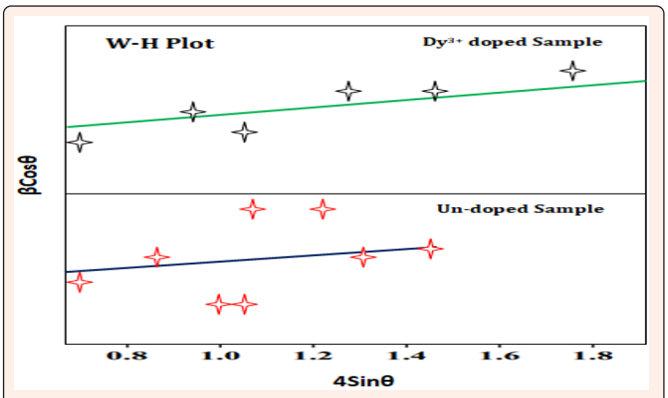

Figure 3: W-H Plot of Un-doped & Dy^{3+} doped Sample

b. **Williamson–Hall (W–H) plot method**

This method is a very important and essential method from the point of view of estimating the crystal lattice strain clearly present in the synthesized samples. In this way, FWHM can be represented as a linear combination of the major role from the crystallite size & crystal lattice strain [23]. Tables 1 & 2 clearly displays the crystalline parameters. The crystallite size and the strain component upsurge with increase in the do-pant ion concentration which raises in turn the volume of the unit cell in the crystal.

$$\beta \cos\theta = \frac{k\lambda}{L} + 4\varepsilon \sin\theta \quad (4)$$

Where, 'β=2(θ2-θ1)'; represents the FWHM (in radians), 'θ' represents the Bragg angle of the peak, 'λ' (i.e. 1.5405Å); represents the wavelength of X-ray wavelength for target Cu-K_α radiation used, 'L'; represents the effective particle size and ' '; represents the effective crystal lattice strain. The determination of the effective particle size [L] for which the crystal lattice strain is taken into account can be the extrapolated from the plot as clearly displayed in Figure 3. The crystal lattice strain was determined from the slope and the crystalline size was determined from the y-intercept of the linear fit. The W-H plots clearly demonstrate that the line extension was essentially isotropic, which represents that the diffraction domains were isotropic and present with a small percentage of microscopic-strain. The average crystallite size calculated with the help of Debye-Scherer's mathematical formula and (W–H) plot method, respectively. It is very clear that the average crystallite size of all synthesized samples was obtained to be maximum calculated by W-H plot method as compared to the Debye scherrer mathematical method. Along with, observation of the values from Table 1 & 2 displays that the average crystallite size and crystal lattice strain size of $Ca_2MgSi_2O_7$: Dy^{3+} Phosphor are maximum compared to the un-doped phosphor.

Table 1: Determination of average crystallite size (L) and average crystal lattice strain (ε) of $Ca_2MgSi_2O_7$ phosphor.

No.	Diffraction Peaks (2θ)	Respective Plane	Crystallite Size (L) Debye Scherrer	Crystallite Size (L) W-H Plot	Crystal Lattice Strain Size (ε)
1	25.13	210	44nm	55nm	0.25nm
2	29.19	201	47nm	56nm	0.24nm
3	31.24	211	52nm	62nm	0.27nm
4	32.75	220	54nm	64nm	0.25nm
5	38.64	102	48nm	57nm	0.24nm
6	44.07	212	46nm	60nm	0.26nm
Average Size			~49nm	~ 59nm	~ 0.25nm

Table 2: Determination of average crystallite size (L) and average crystal lattice strain (ε) of $Ca_2MgSi_2O_7$: Dy^{3+} phosphor.

No.	Diffraction Peaks (2θ)	Respective Plane	Crystallite Size (L) Debye Scherrer	Crystallite Size (L) W-H Plot	Crystal Lattice Strain Size (ε)
1	25.13	210	67nm	72nm	0.25nm
2	29.19	201	68nm	70nm	0.26nm
3	31.24	211	70nm	72nm	0.29nm
4	32.75	220	66nm	69nm	0.27nm
5	38.64	102	67nm	73nm	0.29nm
6	44.07	212	68nm	70nm	0.28nm
Average Size			~ 68nm	~ 71nm	~ 0.27nm

Radius percentage difference: To ensure the substitution of the cation of host crystal lattice sites by trivalent dysprosium (i.e. coordination no. 6) rare-earth do-pant ion is used according to the mathematical relation [Eq. 7], which calculates the ionic-radius percentage difference between the do-pant ion and host crystal lattice site. In this way, an important condition for the substitution of cation by do-pant ion is that the radius percentage difference of the cation must be less than 30% [24]. Therefore, when this happens, the do-pant [Dy^{3+}] ion can very easily substitute the cation [Ca^{2+}] sites.

$$D_r = \frac{[R_m(CN) - R_n(CN)]}{R_m(CN)} \times 100\% \quad (8)$$

Table 3: Radius percentage difference D_r (%) between the Do-Pant and replace cation.

No.	Cation [R_m (CN)]	Do-pant ion [R_n (CN)]	Radius percentage difference D_r (%)
1	Ca^{2+} [1.00 (VI)]	Dy^{3+} [0.912 (VI)]	9
2	Ca^{2+} [1.12 (VIII)]	Dy^{3+} [0.912 (VI)]	19
3	Mg^{2+} [0.72 (IV)]	Dy^{3+} [0.912 (VI)]	-27
4	Si^{4+} [0.40 (IV)]	Dy^{3+} [0.912 (VI)]	-128

The calculated radius percentage difference values of the synthesized doped phosphors are demonstrated in Table 3. From the above discussion it becomes very clear that in the present research work do-pant ion [Dy^{3+}] clearly substitutes the alkaline-earth ion [Ca^{2+}] in host crystal lattice site. It can be supposed that the do-pant Dy^{3+} ion enters in host crystal lattice ($Ca_2MgSi_2O_7$). As a result, it is very clear from Table 1 that the Dy^{3+} ion clearly substitutes the host crystal lattice site of only Ca^{2+} ions. This is mainly due to the ionic radius of Dy^{3+} (VI) ion (0.912 Å) being much closer to Ca^{2+} (VI) ion (about 1.00 Å) and Ca^{2+} (VIII) ion (about 1.12 Å) rather than the ionic radius of Mg^{2+} (IV) ion (about 0.72 Å) as well as ionic radius of Si^{4+} (IV) ion (about 0.40 Å) [25,26]. Here upon, Dy^{3+} ions are more likely to occupy the Ca^{2+} lattice sites in the host crystal lattice (i.e. $Ca_2MgSi_2O_7$) and thus will generate traps in substituted host crystal lattice site because of the different electro-negative tendencies of the two ions. Table 3 confirms that the dysprosium [Dy^{3+}] ions do not completely occupy two other tetrahedral sites, namely magnesium [Mg^{2+}] & silicon [Si^{4+}] ions. Therefore, [Ca^{2+}] lattice sites can occupy two alternative lattice sites, the six coordinated [Ca^{2+}] site [CaO6 (Ca (I) site)] and the eight coordinated [Ca^{2+}] site [CaO8 (Ca (II) site)] [27]. We have also observed that the Mg^{2+} [MgO4], and Si^{4+} [SiO4] also evident, other two independent positive ions (i.e. cation) in the crystal lattice site. Both, [Mg^{2+}] and [Si^{4+}] cations clearly occupy in the tetrahedral lattice sites.

FESEM images and EDX analysis

The surface morphology of the prepared Dy^{3+} doped $Ca_2MgSi_2O_7$ powder sample was clearly analyzed with the help of FESEM image, and it is clearly displayed in Figure 4(a). Analysis of the FESEM image reveals that the sizes of the particles exist in the prepared samples 45-60nm or more. The particles were not uniform, and they were tightly aggregated to each other with different particle size distributions. In addition, due to the high temperature heat treatment, there are some large aggregates are clearly evident in this morphology of the particles. The actual evidence of elements likewise Ca, Mg, Si, O and Dy sharp peaks are clearly present in EDX spectra which preliminary indicates the actual formation of the $Ca_2MgSi_2O_7$:Dy^{3+} sample in Figure 4(b) which confirms doping of Dy^{3+} ions in the $Ca_2MgSi_2O_7$ host crystal lattice. Along with the clear evidence of rare-earth Dysprosium ions in their relevant EDX spectrum image. As such, their EDX spectrum showed no emission peaks other than (Ca) calcium, (Si) silicon, (O) oxygen and Mg (magnesium). In this EDX spectrum, intense peaks of Ca, Si, O, and Dy, are clearly evident which clarifies the existence of these elements of the actual chemical composition in the synthesized phosphor sample with respect to Weight % and Atomic % also analyzed which is displayed in Table 4.

Table 4: Chemical composition of $Ca_2MgSi_2O_7$:Dy^{3+} sample.

No.	Elements	Atomic (%)	Weight (%)
1	O K	43.18	64.18
2	Mg K	5.94	5.79
3	Si K	15.02	12.64
4	Ca L	27.03	16.07
5	Dy L	8.83	1.32
Total		100.00	100.00

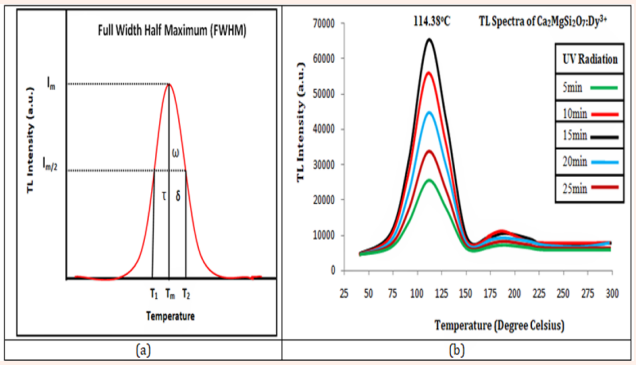

Figure 4: (a) FESEM Image and (b) EDX analysis of synthesized $Ca_2MgSi_2O_7:Dy^{3+}$ phosphor.

Thermoluminescence (TL) analysis

The phenomenon of TL can also be defined in this way that it is one of the most essential technique for making an in-depth study of the trap-centers as well as trap-level in an insulator or semiconductor stimulated by any radiation-source [28,29]. Usually information of trapping level and thermal depth of trap can be obtained by thermo-luminescence curve. A novel TL luminescent material exhibits superior long afterglow characteristics, referred to as persistent luminescence. It is clear from definition that after excitation expulsion, it can persist in blackness for a long-time [30]. As such, they are playing a more essential and important role in various application areas such as brightness in the darkness road, bio-imaging and emergency indication sign, display board, advisory display etc. At present era, the rising of specific TL luminescent material exhibits a modern and rapid flourishing application of many research fields in physics, medicine, mining as well as mineral prospering, forensic science, high temperature radiation dosimetry and archeological dating [31].

Figure 5(b) represents the TL glow curve peak of prepared Dy^{3+} doped $Ca_2MgSi_2O_7$ powder sample for different UV radiation dose times (i.e. 5, 10, 15, 20 and 25min) with a constant heating rate. In our case, while studying these glow curves, we find that the intensity of TL glow curve peak increases with irradiation dose time increasing up to 15 minutes and then decreases with over time afterwards. The main reason for this can be seen that at a specific UV radiation time, the large numbers of trapped electrons in a meta-stable state approaches its optimum values. During observation of the TL glow curve peak of the phosphor sample it is revealed that a single fitted sharp and broad glow peak confirms its existence at 112.38 °C. The respective depth of the trap should be deeper which responsible due to high temperature at 112.38 °C, respectively. Primarily, these deeper traps contribute significantly to the initial intensity of the afterglow process, and are very helpful for increasing the long persistent duration. Deeper the trap depths, longer the time needed to completely release the trapped electrons or holes and longer the afterglow duration is expected. It is clearly evident that the TL data indicate the presence of single trapping levels in sintered phosphor sample which represented only a single glow curve peak. To determine the trapping parameters, the peak shape method Figure 5(a) is being widely utilized. This method is also known as Chen's method. The geometrical shape factor (μg) was determined with following mathematical expression as:

$$\mu_g = \frac{T_2 - T_m}{T_2 - T_1} \quad (9)$$

Where Tm represents optimum temperature which respect to TL glow curve peak, while T^1 and T^2 represents to the full-width at half maxima (FWHM) which respect to TL glow curve peak. The geometric shape factor (μg) of the single glow peaks was obtained between in the range of 0.47-0.48, respectively. It is very clear from observation that these values are near-about to the second-order kinetics (0.49-0.52), which displays that the single band is the second-order peak point. The result signs that the charge carriers (hole or electrons) are released from the traps with respect to the single band. As a consequence, the possibility of release of retrapping charge carriers is highly enhanced as compared to the non first-order kinetics case [32]. It is worth noting that the second order kinetics which supports the maximum probability of re-trapping released charges carriers before recombination mechanism process. According to Sakai's and Mashangva, it is also reported that a trap depth or activation Energy (E) between 0.65-0.75eV is well appropriate for long afterglow properties [33,34]. We propose that this sintered sample is preferable long-persistent phosphor and novel TL material.

Trapping parameters: In this sequence, this analytical peak shape method and the empirical mathematical formulas [Eqns 9-12], which were proposed by Chen and utilized to estimate the following kinetic or trapping parameters like (activation energy (E) or trap depth, order of kinetics (b), frequency factor (s) and lifetime (τ) of TL glow peak curves. All parameters have estimated according to Eqns (9-12).

a) **Traps depth or activation energy (E)**

$$E_\alpha = C_\alpha \left(\frac{kT_m^2}{\alpha} \right) - b_\alpha \left(2kT_m \right) \quad (10)$$

Where, k denotes the Boltzmann constant.

b) **Frequency factor (S)**

The relationship between the frequency factor (s) and the trap-depth or activation energy (E) is given by the following mathematical equation:

$$\frac{\beta E}{kT_m^2} = s \left[1 + (b-1) \frac{2kT_m}{E} \right] \exp\left(-\frac{E}{kT_m} \right) \quad (11)$$

Where, β denotes the heating rate and b denotes the order of the kinetics (in our case b=2).

c) **Lifetime (τ)**

The relationship between the lifetime (τ), frequency factor (s) and the trap-depth or activation energy (E) at temperature (T) is given by the following equation:

$$\tau = s^{-1} \exp\left(\frac{E}{kT} \right) \quad (12)$$

All trapping parameters of TL glow curve peak have evaluated in the room temperature are given in the Table 5. It is clearly evident that as the fixed doping concentration of Dy^{3+} ion increases as well as the relative TL intensity also increases and reaches its optimum value. It is also confirmed that the TL intensity decreases with further increase in concentration of Dy^{3+} ions. As a result, it has found that as the concentration of activator ions increases due to this the distance between the activators ions becomes noticeably smaller. Energy is transferred from one ion to another ion due to increased interaction of the activators ions.

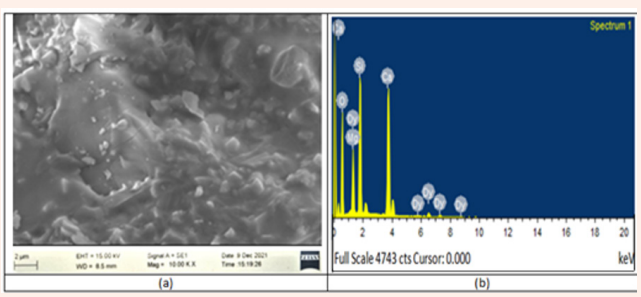

Figure 4: (a) FESEM Image and (b) EDX analysis of synthesized Ca2MgSi2O7:Dy3+ phosphor.

On the other hand, it is also confirmed that the energy stored by the ions decreases with the decrease in the concentration of the activator ions. Consequently, there is an optimum and favorable concentration of the activator ion in synthesized sample at 15min UV- irradiation time. Typically, the trapped electron in the crystal lattice site and the self-trapped hole that are responsible for crystal growth process are firmly connected with the oxygen $[O^{2-}]$ and silicon $[Si^{4+}]$ vacancies generated under it. After the above process, the holes in the crystal lattice site returns to the dysprosium $[Dy^{3+}]$

site via thermal stimulation mechanism and get trapped again, that is, the process of re-trapping takes place. Meanwhile, heating of the phosphor sample leads to de-trapping of the traps. As a result, the radiative recombination mechanism on dysprosium [Dy^{3+}] gives rise to the thermoluminescence (TL) stimulation process. In the case of nano-phosphors, it can be observed that the average mean free path of the de-trapped electrons is of the sequence of the crystal lattice size of a few nanometers range.

Table 5: Kinetic parameters of UV-irradiated $Ca_2MgSi_2O_7:Dy^{3+}$ phosphor.

UV Radiation	Peak temperature (T_m/K)	Activation Energy E (eV)	Frequency Factor S (Hz)	Lifetime τ (s)
5min	387.38	0.65	4.2×10^7	3.8×10^5
10min	387.38	0.70	2.3×10^7	5.4×10^5
15min	387.38	0.70	2.3×10^7	5.4×10^5
20min	387.38	0.64	9.7×10^9	4.3×10^3
25min	387.38	0.62	9.1×10^7	4.7×10^3

Conclusion

Phosphors were successfully synthesized via traditional high temperature solid-state reaction synthesis technique in a weak reducing atmosphere. The synthesized powder sample's crystal phase was identified with the help of XRD analysis and the thermal characteristics were also discussed. The crystallite size and the crystal lattice strain size were obtained to be maximum, which have calculated by W-H plot method as compared to the Debye-Scherrer mathematical method. XRD result have revealed that the synthesized phosphors are crystalline and a single phase tetragonal crystallography with akermanite crystal structure. In the case of TL glow curve, single intense peak were clearly observed at 114.38 °C. The activation energy was obtained in the range between 0.62-0.70eV and lifetime has observed in the range between 3.8×10^5 to 5.4×10^5. The frequency factor has observed in the range between 2.3×10^7 (s^{-1}) to 9.7×10^9 (s-1). The trapped electrons in the crystal lattice site and the self–trapped hole that both are responsible for crystal growth process. Deeper traps are highly helpful for increasing the long persistent duration and afterglow process. Therefore, it is also considered and highly applicable to be a new promising solid-state lighting devices, novel TL material, high temperature radiation dosimetry applications and long persistent phosphor.

Acknowledgement

Authors are very grateful to Dept. of Physics, Dr. Radha Bai, Govt. Navin Girls College, Raipur (C.G) for support in experimental research work. We are also thankful to kind support NIT Raipur (C.G.) and Kalinga University Raipur and Pt. Ravishankar Shukla University, Raipur (C.G.) India. The first author undertakes the work of writing the entire research Paper, data collection, paper design and results-discussion. Similarly, second author has properly checked the spelling mistake and grammatical error and helped in sample preparation.

Authors Contributions

This work was carried out in collaboration between both authors. Author Dr. Shashank Sharma undertakes the manuscript designed and conducted the entire experiments & characterization studies, collected and analyzed the research data, and prepared the entire manuscript draft as well as supervised the results-discussion. Similarly, author Dr. Sanjay Kumar Dubey has properly checked the spelling mistake, punctuation, grammatical error, conceptualization, writing, review, editing and helped in sample preparation. Both authors read and approved the final manuscript.

References

1. Revannasiddappa GR, Basavaraj RB, Rudresha MS, Nagaraju G, Kumar S, et al. (2021) White-light emitting $Ca_2MgSi_2O_7:Dy^{3+}$ nanopowders: Structural, spectroscopic investigations and advanced forensic applications. Vacuum184: 109940.
2. Caracas R, Xavier G (2003) Ab initio determination of the ground-state properties of $Ca_2MgSi_2O_7$ åkermanite. Physical Review B 68(18): 184102.
3. Schaper AK, Schosnig M, Kutoglu A, Treutmann W, Rager H (2001) Transition from the incommensurately modulated structure to the lock-in phase in Co-åkermanite. Acta Crystallographica Section B: Structural Science 57(4): 443-448.
4. Jung KY, Han KH, Kang YC, Jung HK (2006) Preparation of $CaMgSi_2O_6$: Eu blue phosphor particles by spray pyrolysis and its VUV characteristics. Materials Chemistry and Physics 98(2-3): 330-336.
5. Watari T, Tsuji T, Mori K, Luitel HN, Torikai T, et al. (2013) Fabrication and characterization of calcium silicate phosphors-Ca2SiO4 and $Ca_2MgSi_2O_7$. Materials Science Forum 761: 59-64.
6. Nagaraj R, Raja A, Ranjith S (2020) Synthesis and luminescence properties of novel red-emitting Eu^{3+} ions doped silicate phosphors for photonic applications. Journal of Alloys and Compounds 827: 154289.
7. Xu X, Shao Q, Yao L, Dong Y, Jiang J (2020) Highly efficient and thermally stable Cr_3^+-activated silicate phosphors for broadband near-infrared LED applications. Chemical Engineering Journal 383: 123108.
8. Zhang GB, Qi ZM, Zhou HJ, Fu YB, Huo TL, et al. (2005) Photoluminescence of (Eu_2^+-Dy^{3+}) co-doped silicate long lasting phosphors. Journal of Electron Spectroscopy and Related Phenomena 144-147: 861-863.
9. McKeever SWS (2011) Optically stimulated luminescence: A brief overview. Radiat Measurements 45: 1336-1341.
10. Dutczak D, Milbrat A, Katelnikovas A, Meijerink A, Ronda C, et al. (2012) Yellow persistent luminescence of Sr_2SiO_4: Eu_2^+, Dy^{3+}. Journal of Luminescence 132(9): 2398-2403.
11. Luitel HN, Watari T (2016) Color tunable persistent luminescence in $M_2MgSi_2O_7$: Eu_2^+, Dy^{3+} (M= Ca, Sr, Ba) phosphor with controlled microstructure. Journal of Applied Chemical Science International 7(2): 76-83.
12. Cao H, Liu M, Chen H (2019) The luminescent properties of long afterglow phosphors: $Ca_2MgSi_2O_7$: Eu_2^+, Tm^{3+} with different preparation temperatures. Physica B: Condensed Matter 571: 243-246.
13. Shashank S, Dubey SK (2022) Specific role of novel TL material in various favorable applications. Insights in Mining Science & Technology 3(2): 001-009.
14. Shashank S, Dubey SK (2021) The significant properties of silicate based luminescent nanomaterials in various fields of applications: A review. International Journal of Scientific Research in Physics and Applied Sciences 9(4): 37-41.
15. Onani MO, Dejene FB (2014) Photo-luminescent properties of a green or red emitting Tb^{3+} or Eu^{3+} doped calcium magnesium silicate phosphors. Physica B: Condensed Matter 439: 137-140.
16. Gong Y, Wang Y, Xu X, Li Y, Jiang Z (2009) Enhanced long persistence of $Ca_2MgSi_2O_7$: Eu_2^+ yellow-green phosphors by co-doping with Ce^{3+}. Journal of the Electrochemical Society 156(10): J295.
17. Parlinski K, Piekarz P (2021) Ab initio determination of Raman spectra of Mg_2SiO_4 and $Ca_2MgSi_2O_7$ showing mixed modes related to LO/TO splitting. Journal of Raman Spectroscopy 52(7): 1346-1359.
18. JCPDS PDF File No. 17-1149, JCPDS International Center for Diffraction Data.
19. American Mineralogist Crystal Structure Data-Base-Code AMCSD 0008032.
20. Venkataravanappa M, Basavaraj RB, Darshan GP, Prasad BD, Sharma SC, et al. (2018) Multifunctional Dy (III) doped di-calcium silicate array for boosting display and forensic applications. Journal of Rare Earths 36(7): 690-702.
21. Klug HP, Alexander LE (1954) X-ray diffraction procedures. John Willey and Sons, Inc. New York, US. p 512.
22. Mondal K, Manam J (2020) Colour-tunable luminescence and thermal stability of blue-green emitting $Ba_2MgSi_2O_7$: Ce^{3+}, Tb^{3+} phosphors. Journal of Molecular Structure 1215: 128262.
23. Hall WH, Williamson GK (1951) The diffraction pattern of cold worked metals: I The nature of extinction. Proceedings of the Physical Society. Section B 64(11): 937.
24. Kasturi S, Sivakumar V, Varadaraju UV (2017) Synthesis and photoluminescence of Eu (II) in barium zinc orthosilicate: A novel green color emitting phosphor for white-LEDs. Luminescence 32(3): 334-340.

25. Shannon RD (1976) Acta crystallographica section A: crystal physics, diffraction, theoretical and general crystallography 32: 751-67.

26. Sharma S, Dubey SK, Diwakar AK, Pandey S (2021) Novel white light emitting ($Ca_2MgSi_2O_7$: Dy^{3+}) phosphor. Journal of Materials Science Research and Reviews 8(4): 164-171.

27. Jiang L, Chang C, Mao D, Feng C (2003) Concentration quenching of Eu_2^+ in $Ca_2MgSi_2O_7$: Eu_2^+ phosphor. Materials Science and Engineering: B 103(3): 271-275.

28. Murthy KVR, Reddy JN (2008) Thermoluminescence: Basic theory, applications and experiments. Nucleonix Systems Pvt. Ltd., Hyderabad, India.

29. Vij DR (1993) Thermoluminescence materials. PTR Prentice-Hall, Inc. A Simon a Schuster Company, Englewood Cliffs, New Jersey, US, p. 7632.

30. Lin L, Zhao Z, Zhang W, Zheng Z, Yin M (2009) Photo-luminescence properties and thermo-luminescence curve analysis of a new white long-lasting phosphor: $Ca_2MgSi_2O_7$:Dy^{3+}. Journal of rare Earths 27(5): 749-752.

31. Kiisk V (2013) Deconvolution and simulation of thermoluminescence glow curves with Mathcad. Radiation Protection Dosimetry 156(3): 261-267.

32. Mc Keever SWS (1985) Thermoluminescence of solids. London: Cambridge University Press, UK.

33. Mashangva M, Singh MN, Singh TB (2011) Estimation of optimal trapping parameters relevant to persistent luminescence. Indian Journal of Pure & Applied Physics 49: 583-589.

34. Sakai R, Katsumata T, Komuro S, Morikawa T (1999) Effect of composition on the phosphorescence from $BaAl_2O_4$: Eu_2^+, Dy^{3+} crystals. Journal of luminescence 85(1-3):149-154.